



Comparison of Americium(III) and Neodymium(III) Monothiophosphate Complexes

May 2024

Changing the World's Energy Future

Thomas Edward Schoenzart, Gregory Peter Holmbeck, Thomas E. Albrecht-Schnzart, Daniela Gomez Martinez, Joseph M. Sperling, Nicholas B. Beck, Hannah B. Wineinger, Jacob P. Brannon, Megan A. Whitefoot



DISCLAIMER

This information was prepared as an account of work sponsored by an agency of the U.S. Government. Neither the U.S. Government nor any agency thereof, nor any of their employees, makes any warranty, expressed or implied, or assumes any legal liability or responsibility for the accuracy, completeness, or usefulness, of any information, apparatus, product, or process disclosed, or represents that its use would not infringe privately owned rights. References herein to any specific commercial product, process, or service by trade name, trade mark, manufacturer, or otherwise, does not necessarily constitute or imply its endorsement, recommendation, or favoring by the U.S. Government or any agency thereof. The views and opinions of authors expressed herein do not necessarily state or reflect those of the U.S. Government or any agency thereof.

Comparison of Americium(III) and Neodymium(III) Monothiophosphate Complexes

Thomas Edward Schoenzart, Gregory Peter Holmbeck, Thomas E. Albrecht-Schnzart, Daniela Gomez Martinez, Joseph M. Sperling, Nicholas B. Beck, Hannah B. Wineinger, Jacob P. Brannon, Megan A. Whitefoot

May 2024

**Idaho National Laboratory
Idaho Falls, Idaho 83415**

<http://www.inl.gov>

**Prepared for the
U.S. Department of Energy
Under DOE Idaho Operations Office
Contract DE-AC07-05ID14517**

Comparison of Americium(III) and Neodymium(III) Monothiophosphate Complexes

Daniela Gomez Martinez,¹ Joseph M. Sperling,¹ Nicholas B. Beck,¹ Hannah B. Wineinger,¹ Jacob P. Brannon,¹ Megan A. Whitefoot,¹ Gregory P. Horne,² Thomas E. Albrecht-Schönzart^{1,2*}

¹Department of Chemistry and Nuclear Science and Engineering Center, Colorado School of Mines, Golden, CO 80401, USA

²Center for Radiation Chemistry Research, Idaho National Laboratory, Idaho Falls, ID, P.O. Box 1625, 83415, USA

*Corresponding author email: tschoenzart@mines.edu

Abstract

Mixed-donor ligands, such as those containing a combination of O/N or O/S, have been studied extensively for the selective extraction of trivalent actinides, especially Am³⁺ and Cm³⁺, from lanthanides during the recycling of used nuclear fuel. Oxygen/sulfur donor ligand combinations also result from the hydrolytic and/or radiolytic degradation of dithiophosphates, such as the Cyanex[®] class of extractants, that are initially converted to monothiophosphates. To understand potential differences between the binding of such degraded ligands to Nd³⁺ and Am³⁺, the monothiophosphate complexes [M(OPS(OEt)₂)₅(H₂O)₂]²⁻ (M³⁺ = Nd³⁺, Am³⁺) were prepared and characterized by single crystal X-ray diffraction and optical spectroscopy and studied as a function of pressure up ca. 14 GPa using diamond-anvil techniques. Although Nd³⁺ and Am³⁺ have nearly identical eight-coordinated ionic radii, these structures reveal that while the M–O bond distances in these complexes are nearly equal that the M–S distances are statistically different. Moreover, for [Nd(OPS(OEt)₂)₅(H₂O)₂]²⁻, the hypersensitive ⁴I_{9/2}→⁴G_{5/2} transition shifts as a function of pressure by –11 cm⁻¹/GPa. Whereas for [Am(OPS(OEt)₂)₅(H₂O)₂]²⁻, the ⁷F₀→⁷F₆ transition shows a slightly stronger pressure dependence with a shift of –13 cm⁻¹/GPa and also exhibits broadening of the 5*f*→5*f* transitions at high pressures. These data likely indicate

an increased involvement of the $5f$ orbitals in bonding to Am^{3+} relative to that of Nd^{3+} in these complexes.

Introduction

Increasing energy demands and the heightened effects of global climate change have led to a renewed interest in nuclear energy because of its low CO_2 emissions and high energy density.^{1,2} When low-enriched uranium fuel is fissioned only *ca.* 1% of the available energy is accessed before fission products that act as neutron poisons (*e.g.* ^{157}Gd) build up in the fuel and necessitate its replacement in the reactor.³ Recycling used nuclear fuel requires separating the neutron-capture products americium and curium from lanthanide fission products.⁴⁻⁸ However, post-plutonium actinide elements such as americium and curium possess redox potentials that are similar to many lanthanides and are thus dominated by the $3+$ oxidation state. Owing to overlapping ionic radii and the lack of easily accessible redox manipulations, the separation of An(III) cations from Ln(III) cations has been a long-standing problem that hampers developing closed nuclear fuel cycles.^{6,7,9,10}

Notably ^{241}Am can be fissioned in fast neutron spectrum reactors to reduce the heat load, footprint, and long-term radiotoxicity that it would pose on nuclear waste repositories.⁹ In contrast, the need to separate curium stems from the relatively high spontaneous fission rate of ^{244}Cm and the hazards associated with the concomitant production of neutrons.¹¹ While many successful strategies have been developed for $\text{Am}^{3+}/\text{Cm}^{3+}$ and $\text{An}^{3+}/\text{Ln}^{3+}$ separations including ion-exchange chromatography and liquid-liquid extraction,^{6,7} these methods are affected by the high radiation fields that are present when used nuclear fuel is being processed.^{8,10,12} Radiolytic and hydrolytic reactions degrade extractants and resins affecting the efficiency of the processes and can even lead to the formation of deleterious products such as the low-solubility plutonium

dibutylphosphates that can form during the PUREX process.^{13,14}

Liquid-liquid extraction systems for the recovery of the so-called minor actinides (Np, Am, Cm) from used nuclear fuel can be classified into two categories. The first category is based on extractants that coextract lanthanides and actinides. The second category is based on only recovering actinides.¹² The former extractants typically coordinate metal cations using oxygen donor atoms or ions. These include, but are not limited to, phosphine oxides, carbamoylphosphine oxides, organophosphoric acids, malonamides, and diglycolamides.¹² Bidentate ligands with hard oxygen donor atoms such as *N, N, N', N'*-tetraoctyl-3-oxapentane-1,5-diamide (TODGA) and octylphenyl-*N,N*-diisobutyl methylene carbamoyl phosphine oxide (CMPO) can coextract trivalent lanthanides and actinides from high-level liquid waste solutions in a highly efficient manner.^{12,15,16}

Selectivity for An(III) cations over Ln(III) cations usually relies on differences in the enthalpies of binding to relatively soft nitrogen- or sulfur-donor ligands versus the aforementioned oxygen-donor ligands.^{15,17-23} Examples of such soft-donor systems include the pure N-donor ligand bis(triazinyl)pyridine (BTP)^{9,24} and the aforementioned dithiophosphates; both of which have shown high selectivity for Am(III) over Ln(III) cations. Bidentate dithiophosphinic acids were one of the first types of ligand to show high selectivity for actinides over lanthanides.^{16,25,26} Synergistic mixtures such as di-2-ethylhexyl dithiophosphoric acid (HDEHDTP) with tributylphosphate (TBP) provides a separation factor of 60 for Am(III) over Eu(III).²⁷ Likewise, mixtures of bis(4-chlorophenyl)dithiophosphinic acid and tris(2-ethylhexyl)phosphate have been shown to have separation factors over 3000 for Am(III) and Cm(III) from the lanthanides.¹⁶ The ligand bis(2,4,4-trimethylpentyl)dithiophosphinic acid (Cyanex 301) is preferred among sulfur-donor ligands because of its selectivity that is increased further in the presence of N-donor neutral ligands.^{24,25,27} Again, dithiophosphates undergo rapid

degradation in the high nitric acid concentrations that are used in spent nuclear fuel recycling and first degrade to monothiodialkylphosphates and then to dialkylphosphates.²⁸ This conversion from a soft-donor donor extractant to a hard-donor ligand results in loss of selectivity for Am(III) over the lanthanides.

Given the importance of the transformation of dithiophosphates to monothiophosphates, it is necessary to detail the origin of the loss of selectivity for An(III) cations that can be addressed, in part, through precise studies of the coordination chemistry of this class of ligands to An(III) and Ln(III) cations. Previous work addressing the coordination of dialkylphosphates, dithiophosphates, and monothiophosphates to *f*-block metal ions includes the synthesis and characterization of *O,O'*-diethyldithiophosphate complexes of La^{III}, Nd^{III}, Sm^{III}, Er^{III}, and Am^{III},²⁹⁻³¹ lanthanide complexes of [OPS(C₆H₁₁)₂]¹⁻, [OPS(CH₃)₂]¹⁻, and Th^{IV} and U^{IV} complexes of [OPS(CH₃)₂]¹⁻, [OPSPH₂]¹⁻, and [S₂P(CH₃)₂]¹⁻.³²⁻³⁵ In contrast, the mixed-donor ligand *O,O'*- diethylmonothiophosphate has not been characterized in the solid state with lanthanides or actinides and only with a small number of transition metals (Mo, Zn and Pt) despite being commercially available.³⁶⁻³⁹ In this present study, we examine the structures and optical properties of [M(OPS(OEt)₂)₅(H₂O)₂]²⁻ (M³⁺ = Nd³⁺, Am³⁺) including the effects of high pressures on these complexes.

Experimental

Caution! ²⁴³Am (*t*_{1/2} = 7,364 years; specific activity 0.2 mCi/mg) is a strong α- and γ-emitter making it an internal and external radiological hazard. ²⁴³Am reaches secular equilibrium with its daughter ²³⁹Np (*t*_{1/2} = 2.356 days; specific activity = 232 Ci/mg) within two weeks, doubling the activity of the material used in these experiments. These studies were carried out in a Category II nuclear hazard facility using carefully executed and choreographed procedures.

Materials. KOPS(OEt)₂ (98%, Sigma-Aldrich), ethyl alcohol, pure (ACS reagent, ≥99.5%, Sigma-Aldrich), dichloromethane (ACS reagent, ≥99.5%, Sigma-Aldrich, DCM), HCl_(aq) (ACS reagent 37%, Sigma-Aldrich), pentane (reagent grade, 98%, Sigma-Aldrich), and Nd₂O₃ (99%, Sigma-Aldrich) were all used as received. ²⁴³Am was supplied by the Radiochemical Engineering Development Center in Oak Ridge National Lab. The Am^{III} stock solution was purified according to literature.⁴⁰NdCl₃·6H₂O was prepared by the dissolution of Nd₂O₃ in concentrated HCl followed by fuming under a gentle stream of nitrogen.

Synthesis

K₂[²⁴³Am(OPS(OEt)₂)₅(H₂O)₂]·CH₂Cl₂·H₂O (Am1): From an aqueous stock solution of ²⁴³Am³⁺ in 2 M HCl, an aliquot of 2.5 mL (5 mg, 0.021 mmol; Am content) was transferred to a 20 mL scintillation vial and dried to a residue with nitrogen and heat. The hydrated AmCl₃·*n*H₂O residue was then dissolved in EtOH (0.5 mL). KOPS(OEt)₂ (17.2 mg, 0.082 mmol) was dissolved in EtOH (0.5 mL) in a 20 mL scintillation vial while stirring at 60 °C. The solution containing the americium material was added dropwise to the solution containing KOPS(OEt)₂. The vial was then capped and left to stir for one hour at 60 °C. After stirring, the solution was dried to a residue with a slow stream of nitrogen. Dichloromethane (1 mL) was added to the vial, dissolving the product. To remove the KCl solid byproduct, the dichloromethane solution was filtered through a glass pipet packed with glass filter paper into a 4 mL shell vial. Vapor diffusion set at room temperature overnight with pentane (3 mL) resulted in peach-colored crystals of **Am1** (18.8 mg/0.0144 mmol, ~70% based on Am metal content).

K₂[Nd(OPS(OEt)₂)₅(H₂O)₂]·CH₂Cl₂·H₂O (Nd1): Like **Am1**, NdCl₃·6H₂O (12.4 mg, 0.0347 mmol) was dissolved in EtOH (0.5 mL). KOPS(OEt)₂ (28.9 mg, 0.139 mmol) was dissolved in EtOH (0.5 mL) while stirring at 60 °C. The NdCl₃·6H₂O solution was added dropwise to the KOPS(OEt)₂ solution. Once the Nd³⁺ solution was added, the vial was capped

and left to stir for one hour at 60 °C. The solution was then dried to a residue by applying a slow stream of nitrogen. Dichloromethane (1 mL) was added to dissolve the product. The vial was washed with dichloromethane (~1 mL) and was filtered through a glass pipet packed with glass fiber filter to remove the KCl. Vapor diffusion of pentane (5 mL) overnight at room temperature resulted in a crop of blue crystals of **Nd1** (23.3 mg/ 0.0193 mmol, ~56% based on Nd metal content).

Crystallographic studies

Single crystals of **Nd1** and **Am1** were placed in immersion oil and carefully mounted on a 75 μm diameter MiTeGen loop with the help of a microscope. The loop was placed on the goniometer of a Bruker D8 Quest X-ray diffractometer. The crystals were centered using a digital camera controlled by the ApexIV software. Collection strategies were calculated and optimized with the ApexIV software. A full sphere of data was collected with an X-ray source with Mo K_{α} radiation ($\lambda = 0.71093 \text{ \AA}$) as the incident beam, and the X-ray scattering was detected with a Photon III detector. The diffraction was collected at 100 K with a Cryo Industries, Cryocool cold stream system. The data was integrated and refined with direct methods using the SHELXTL suite in the OLEX2GUI.^{41,42} The scattering factors for americium were added manually in the instruction file using the SFAC instruction card.⁴³ One of the ethyl groups on one of the $[\text{OPS}(\text{OEt})_2]^{1-}$ ligands is disordered over two positions and is modeled appropriately in both structures. Crystal structures of **Am1** and **Nd1** were submitted to the CCDC with deposition numbers 2301779 and 2301780.

Solid State UV-vis-NIR Spectroscopy

Crystals were placed on a glass slide with immersion oil and UV-vis-NIR transmission data were collected using a CRAIC Technologies Microspectrophotometer. Data was collected

from 320 nm to 1700 nm with data integration times set by the CRAIC software.

Variable Pressure UV-vis-NIR Spectroscopy

Pressure-dependent spectroscopy was performed by placing ruby spheres and a single crystal in a stainless-steel gasket indented to 100 μm with a 200 μm diameter hole drilled through the center mounted in an Almax easyLab TozerDAC diamond anvil cell. Polydimethylsiloxane was used as the pressure medium to ensure hydrostatic pressure and the ruby spheres were used to determine the pressure with the ruby pressure scale.^{44,45} The peak positions were fit using a Voigt function.

Results and Discussion

Synthesis and Structure

$\text{K}_2[\text{Am}(\text{OPS}(\text{OEt})_2)_5(\text{H}_2\text{O})_2] \cdot \text{CH}_2\text{Cl}_2 \cdot \text{H}_2\text{O}$ (**Am1**) and $\text{K}_2[\text{Nd}(\text{OPS}(\text{OEt})_2)_5(\text{H}_2\text{O})_2] \cdot \text{CH}_2\text{Cl}_2 \cdot \text{H}_2\text{O}$ (**Nd1**) can be crystallized through the vapor diffusion of pentane into a dichloromethane solution of either complex and yield high-quality crystals overnight. Single crystal X-ray diffraction studies reveals that they crystallize in the monoclinic space group $P2_1/c$. Am(III) and Nd(III) have ionic radii that are within statistical error of one another (8 coordinate, 1.108(4) Å and 1.107 Å, respectively)^{46,46-48} and the formation of similar or isomorphous compounds is not surprising.^{29,49-62} The formula of **Nd1** and **Am1** are identical, which along with the lattice parameters, symmetry, and atomic coordinates indicates that the compounds are isomorphous. The structures, however, contain small, solvent-accessible voids that for **Nd1** and **Am1** are found to contain disordered water molecules and a dichloromethane molecule. An examination of multiple crystals from different crystallizations of **Nd1** reveals that there can be up to two co-crystallized water molecules per formula unit. However, **Nd1** (and

possibly **Am1**) rapidly dehydrate upon removal from the mother liquor. The water molecules are in small voids that have little to no effect on the overall packing, that is why their removal has no detectable effects on the overall structure. The two structures reported herein were selected from other datasets because they have the highest resolution of the crystals examined.

Both metal centers in the **Am1** and **Nd1** structures are coordinated by two water molecules, four monodentate (κ -O) ligands, and one bidentate (κ -O,S) [OPS(OEt)₂]⁻ ligand adding to a total coordination number of eight as shown in Figures 1 and 2. Both metal centers have a distorted bicapped trigonal prismatic geometry as determined by SHAPES software.⁶³

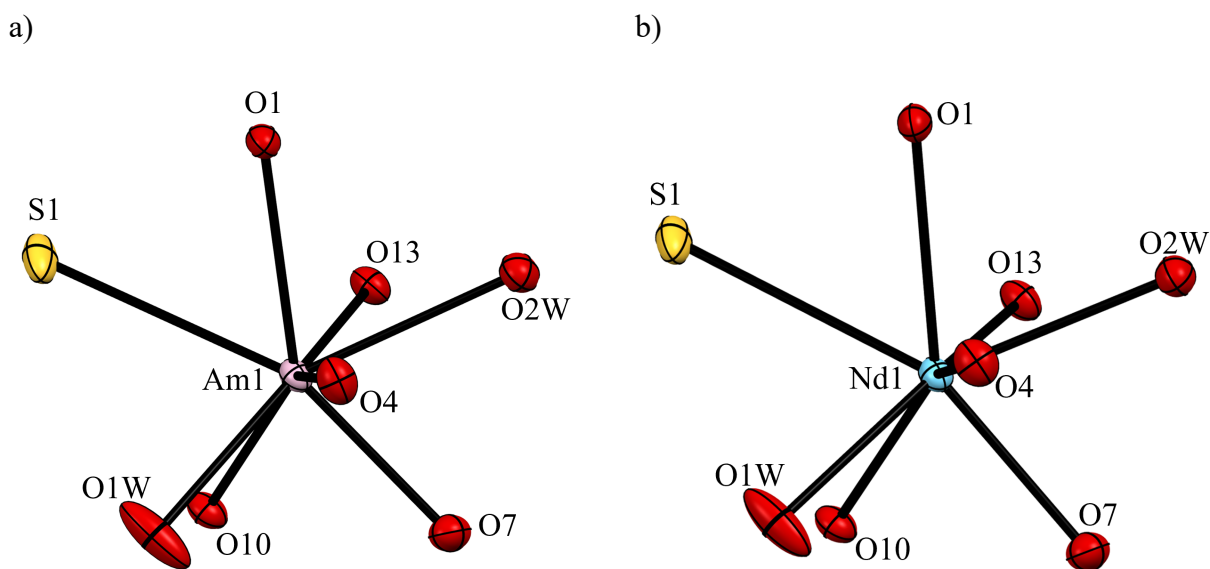


Figure 1. Thermal ellipsoid plots drawn at 50% probability at 100 K showing the coordination environment for a) $\text{K}_2[\text{Am}(\text{OPS}(\text{OEt})_2)_5(\text{H}_2\text{O})_2] \cdot \text{CH}_2\text{Cl}_2 \cdot \text{H}_2\text{O}$ (**Am1**) and b) $\text{K}_2[\text{Nd}(\text{OPS}(\text{OEt})_2)_5(\text{H}_2\text{O})_2] \cdot \text{CH}_2\text{Cl}_2 \cdot \text{H}_2\text{O}$ (**Nd1**).

b)

a)

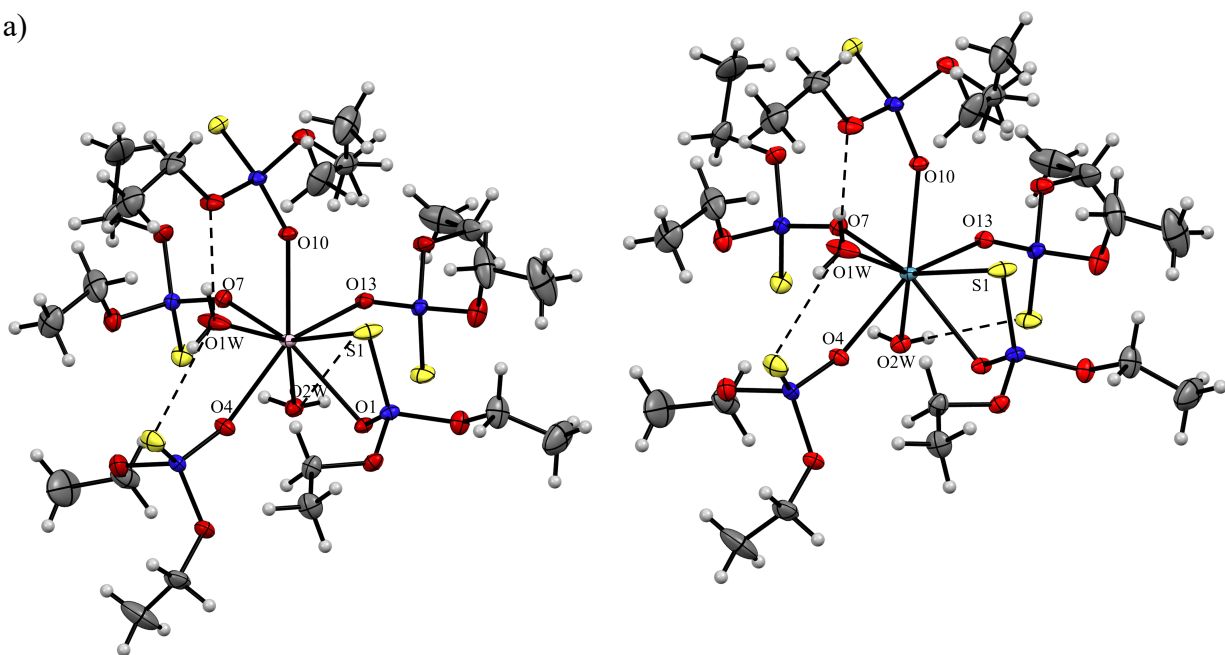


Figure 2. Thermal ellipsoid structure for a) $\text{K}_2[\text{Am}(\text{OPS}(\text{OEt})_2)_5(\text{H}_2\text{O})_2] \cdot \text{CH}_2\text{Cl}_2 \cdot \text{H}_2\text{O}$ (**Am1**) and b) $\text{K}_2[\text{Nd}(\text{OPS}(\text{OEt})_2)_5(\text{H}_2\text{O})_2] \cdot \text{CH}_2\text{Cl}_2 \cdot \text{H}_2\text{O}$ (**Nd1**). Dashed lines are added to show the hydrogen bonding present. Potassium ions and dichloromethane molecules are omitted for clarity. Gray represents carbon, red is oxygen, dark blue is phosphorus, and yellow is sulfur.

For both structures there are two potassium ions balancing the charge of the $[\text{M}(\text{OPS}(\text{OEt})_2)_5(\text{H}_2\text{O})_2]^{2-}$ complex. Seven oxygen atoms and one sulfur atom form the coordination sphere of the K^+ cations. The Am–S bond (2.975(3) Å) in **Am1** is slightly longer in comparison to other compounds containing Am^{III}–S bonds. Other reported Am^{III}–S bond lengths are: Am(2,2'-bipyridine)tris(diethyldithiocarbamate) (2.875(1) Å);⁶⁴ Am(S₂CNEt₂)₃(N₂C₁₂H₈) (2.87(5) Å);⁴⁰ Am(mpo)₂(μ-O-mpo)(H₂O)]₂·3H₂O (mpo[−]= 2-mercaptopyridine N-oxide, 2.903(2) Å);⁶² [Ph₄As][Am(S₂P(OEt)₂)₄] (2.9116(8) Å);²⁹ and [NBu₄][Am^{III}[S₂P(^tBu₂C₁₂H₆)₄] (2.921(9) Å).⁵⁰ The deviation between the later complexes and $[\text{Am}(\text{OPS}(\text{OEt})_2)_5(\text{H}_2\text{O})_2]^{2-}$ of ~ 0.1 Å points to the negative charge of the $[\text{OPS}(\text{OEt})_2]^{1-}$ anion primarily residing on the terminal P–O moiety rather than the P=S unit that could be predicted based on differences in electronegativity. The average P=S bond length in [Ph₄As][Am(S₂P(OEt)₂)₄] is 1.97(1) Å while the P=S bond length for **Am1** is 1.95(1) Å.

The coordination environment of **Am1** has noticeable differences with that of $[\text{Am}(\text{S}_2\text{P}(\text{OEt})_2)_4]^{1-}$.²⁹ $[\text{Am}(\text{S}_2\text{P}(\text{OEt})_2)_4]^{1-}$ has four ligands binding through the sulfur atoms in a bidentate manner adding to a total coordination of eight; resulting in a slightly distorted snub dodecahedron D_{2d} . **Am1** instead has four monodentate ligands binding through the oxygen atoms and one bidentate ligand binding through the oxygen and sulfur in addition to two water molecules, also adding to a total coordination number of eight to yield a distorted bicapped trigonal prismatic geometry with approximate C_{2v} symmetry. The capping atoms are O13 and O1W. The average for the OPS angle in the monothiophosphate structure is $112.2(1)^\circ$ and for the SPS angle in the dithiophosphate structure is $112.39(5)^\circ$.

The average M–O bond length for **Am1** is $2.451(7)$ Å and $2.450(5)$ Å for **Nd1**, respectively. The M–S bonds, however, are statistically different ($\geq 3\sigma$) from one another as provided in Table 1. In **Am1**, the Am–S bond length is $2.975(3)$ Å. Whereas in **Nd1**, the Nd–S bond length is $3.000(2)$ Å. The difference between the two bond lengths is *ca.* 0.025 Å, suggesting a stronger interaction with Am^{III} over Nd^{III} . A similar distance is observed in the Am^{III} bis(triazinyl)pyridine complex $[\text{Am}(\text{EtBTP})_3][\text{BPh}_4]_3 \cdot 3\text{CH}_3\text{CN}$ (EtBTP: 2,6-bis(5,6-diethyl-1,2,4-triazin-3-yl)pyridine); the Am–N bond length was found to be shorter in comparison to the Nd–N bond length.⁵⁴ Electronic structure calculations revealed that this was due to enhanced metal-ligand bonding through π -backbonding in the americium complex that is absent in the neodymium complex.⁵⁴ Additionally, Prüßmann *et al.* showed that N-donor ligands such as 2,6-bis(5,6-dipropyl-1,2,4-triazin-3-yl)pyridine bind preferentially to trivalent actinides over trivalent lanthanides in solution with separation factors ($\text{SF} = D_{\text{Am}}/D_{\text{Eu}}$) greater than 100.⁶⁵ Quantum mechanical calculations and ligand K-edge XANES measurements have revealed that origin of this lies in a greater degree of orbital mixing in the An–L bonds than measured for corresponding Ln–L interactions.

Table 1. Bond lengths (in Å) for **Am1** and **Nd1** with M–S1 bond lengths shaded.

Bond	Am1	Nd1
M-O1	2.562(6)	2.559(6)
M-O4	2.398(9)	2.396(6)
M-O7	2.335(9)	2.336(6)
M-O10	2.443(6)	2.444(3)
M-O13	2.340(9)	2.339(6)
M-O1W	2.45(1)	2.450(6)
M-O2W	2.625(6)	2.621(6)
M-S1	2.975(3)	3.000(2)

Absorption Spectroscopy

Solid-state absorption spectra were collected at room temperature for **Am1** and **Nd1** as shown in Figures 3 and 4, and at $-180\text{ }^{\circ}\text{C}$ for **Am1** (see Figures S16-18). Solution absorption spectra were also collected at room temperature for **Am1** and **Nd1** in dichloromethane (see Figures S14 and S15). The **Am1** spectrum has characteristic $5f \rightarrow 5f$ Laporte forbidden transitions that are indicative of americium(III).^{66,67} The most intense peaks are the Group H transitions (5L_6) at 19725 cm^{-1} (506 nm) and Group E transitions (7F_6) at 12261 cm^{-1} (815 nm). Peaks from Groups A (7F_0 , 7F_1 , 7F_2 ; 6061 cm^{-1}), C (7F_4 ; 9608 cm^{-1}), D (7F_5 ; 11178 cm^{-1}), I (5D_2 ; 21676 cm^{-1}), K (5H_7 ; 23411 cm^{-1}), and M (5G_4 ; 26351 cm^{-1}) are also observed. Groups F and G are weak transitions seen in the region $\sim 13000\text{--}19000\text{ cm}^{-1}$ and were not observed in the spectra collected.⁶⁶ The transition energies for the **Am1** spectrum are similar to other americium complexes with sulfur donor ligands; the Laporte forbidden transitions are around the same

wavelengths with shifting of around 5 cm^{-1} or less.^{29,40,50} In **Am1**, the splitting of the 506 nm peak is more pronounced than in $[\text{Am}(\text{S}_2\text{P}(\text{OEt})_2)_4]^{1-}$, and the splitting in the 815 nm peak is more pronounced in $[\text{Am}(\text{S}_2\text{P}(\text{OEt})_2)_4]^{1-}$.²⁹ The ratio of those two peaks in the **Am1** spectra is larger than the ratio of the same peaks in $[\text{Am}(\text{S}_2\text{P}(\text{OEt})_2)_4]^{1-}$.²⁹

The **Nd1** spectrum has $4f \rightarrow 4f$ Laporte forbidden transitions that are characteristic of Nd(III).⁶⁸ The most intense peak at 17232 cm^{-1} (580 nm) is the hypersensitive transition $^4\text{I}_{9/2} \rightarrow (^4\text{G}_{5/2}, ^2\text{G}_{7/2})$.⁶⁹ The second most intense peaks are at 13385 cm^{-1} (747 nm) and 12452 cm^{-1} (803 nm) and correspond to the $^4\text{I}_{9/2} \rightarrow (^4\text{F}_{7/2}, ^4\text{S}_{3/2})$ and the $^4\text{I}_{9/2} \rightarrow (^2\text{H}_{9/2}, ^4\text{F}_{5/2})$ transitions, respectively. There is a weak transition at 23236 cm^{-1} (430 nm) corresponding to $^4\text{I}_{9/2} \rightarrow ^2\text{P}_{1/2}$. Other transitions include 21821 cm^{-1} ($^4\text{I}_{9/2} \rightarrow (^2\text{K}_{15/2}, ^4\text{G}_{11/2})$), 21204 cm^{-1} ($^4\text{I}_{9/2} \rightarrow ^2\text{D}_{3/2}$), 20904 cm^{-1} ($^4\text{I}_{9/2} \rightarrow ^2\text{G}_{9/2}$), 19429 cm^{-1} ($^4\text{I}_{9/2} \rightarrow (^4\text{G}_{9/2}, ^2\text{K}_{13/2})$), 19023 cm^{-1} ($^4\text{I}_{9/2} \rightarrow ^4\text{G}_{7/2}$), and 11479 cm^{-1} ($^4\text{I}_{9/2} \rightarrow ^4\text{F}_{3/2}$). In **Nd1**, the splitting in the peak at 580 nm is slightly more pronounced than in $[\text{Nd}(\text{S}_2\text{P}(\text{OEt})_2)_4]^{1-}$. The peaks at 747 nm and 803 nm have a molar absorptivity than the peaks in the $[\text{Nd}(\text{S}_2\text{P}(\text{OEt})_2)_4]^{1-}$ spectrum. This makes the ratio between the 580 nm and 747 nm or 803 nm peak smaller in comparison to $[\text{Nd}(\text{S}_2\text{P}(\text{OEt})_2)_4]^{1-}$.²⁹

Comparing the solid-state and solution phase spectra for both compounds shows that there is no evident shifting of the peak positions between the solid state and solution (see Figures S17 and S18). The solid-state spectra for both compounds have better resolution of splitting than the solution phase. The reduced resolution of peak splitting in solution likely results from ligand fluxations.^{70,71} In **Am1**, this is noted in the 506 and 815 nm peaks. In the solid-state spectrum, the 506 nm peak (Group H) is split into four peaks and has a higher intensity. The 815 nm peak (Group E) is split into two peaks and this attributed to an overlap of the transitions with $J = 5$ and $J = 6$ levels.⁶⁶ In the solution phase, the peaks are broader and coalesce into one signal. For **Nd1**, more splitting is observed in the peaks at 580 and 871 nm in comparison to the solution phase.

This is not the case for the other peaks, where no notable differences are observed in the splitting or sharpness of the transitions.

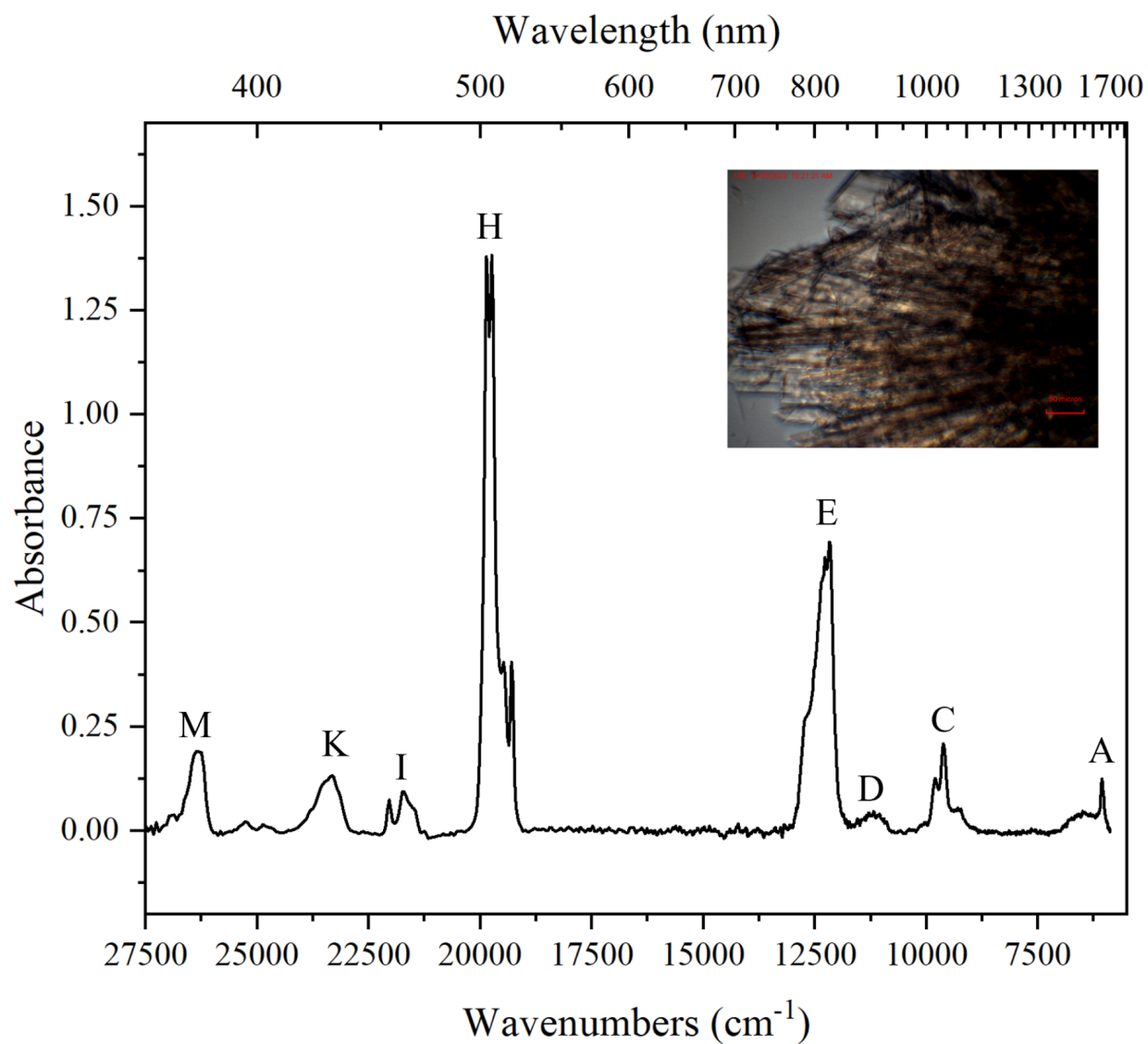


Figure 3. Solid-state UV-vis-NIR absorption spectrum of $\text{K}_2[\text{Am}(\text{OPS}(\text{OEt})_2)_5(\text{H}_2\text{O})_2] \cdot \text{CH}_2\text{Cl}_2 \cdot \text{H}_2\text{O}$ (**Am1**) collected at room temperature with a picture of the crystals and line groups added for clarity.

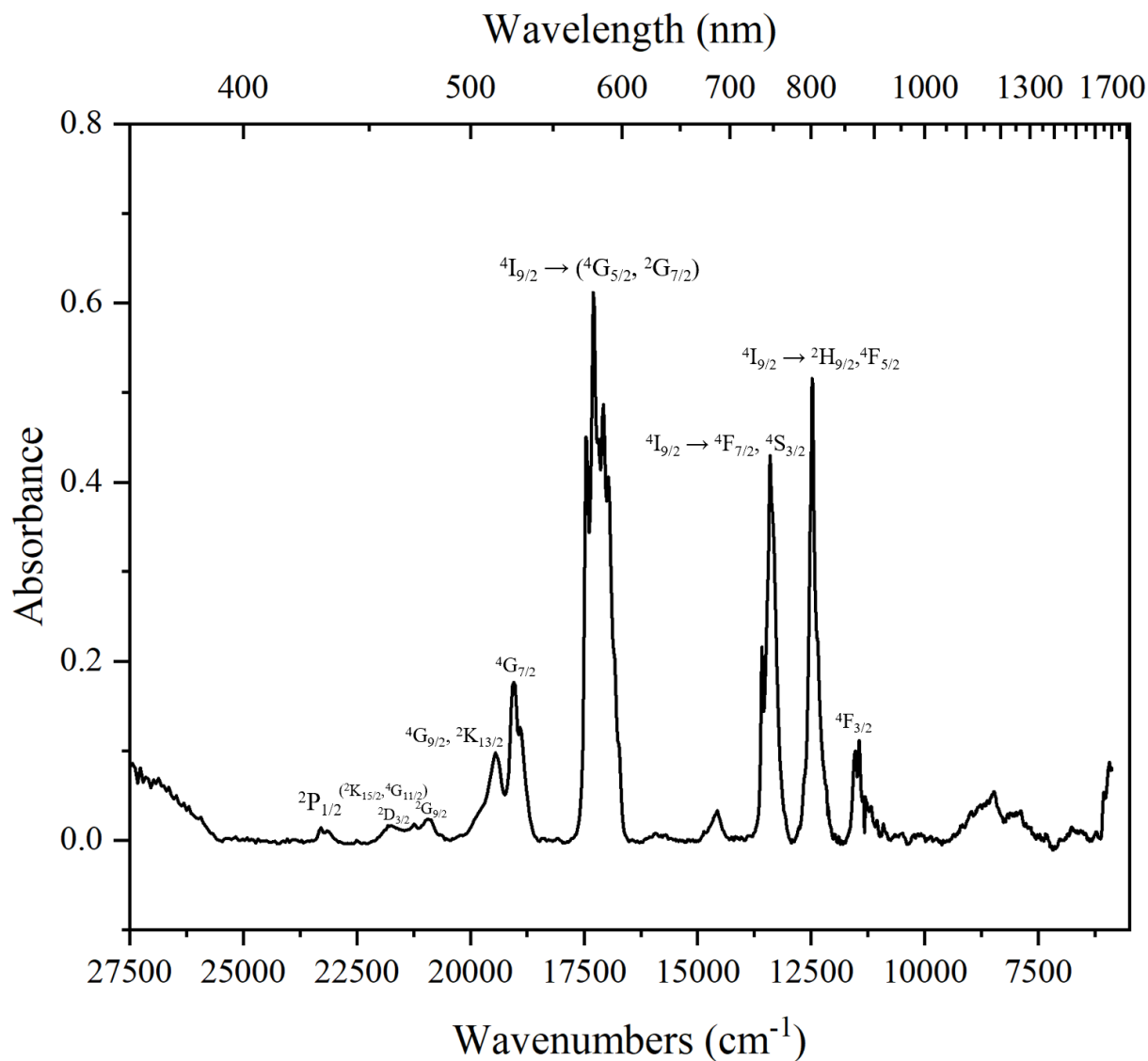


Figure 4. Solid-state UV-vis-NIR absorption spectrum of $\text{K}_2[\text{Nd}(\text{OPS}(\text{OEt})_2)_5(\text{H}_2\text{O})_2] \cdot \text{CH}_2\text{Cl}_2 \cdot \text{H}_2\text{O}$ (**Nd1**) measured at 22 °C.

High-Pressure UV-vis-NIR Spectroscopy

The pressure-dependent spectroscopy of **Am1** and **Nd1** up to 13.91 GPa are shown in Figures 5 and S8, respectively. Because the optical spectra for both metal ions consist primarily of $f \rightarrow f$ transitions, changes in the peak positions and shapes as a function of pressure can be

reflective of changes in the ligand field and/or increased involvement of the *f*-orbitals in forming chemical bonds.^{72–74} The trend that has been observed thus far for Am^{III} coordination compounds is that the largest shifts occur with soft-donor ligands, such as those containing sulfide, that are also delocalized. Thus, [Am(OPS(OEt)₂)₅(H₂O)₂]²⁻ provides an opportunity to investigate a quite different S-donor ligand because in this ligand the negative charge is largely localized on the terminal phosphate oxo atom, and, as previously mentioned, the Am–S bond distance is considerably longer (~0.25 Å) than found in dithiocarbamate complexes, for example.⁴⁰ The rather long Am–S bond distance of 2.975(3) Å, while statistically shorter than that found in the Nd^{III} analog, is nevertheless beyond the limit for 5*f*/3*p* hybridization. Thus, the prediction is that the pressure response for [Am(OPS(OEt)₂)₅(H₂O)₂]²⁻ is likely more similar to that measured in Nd^{III} complexes than determined for Am^{III} complexes with more sulfide-like coordinating ligands.

For **Am1**, several transitions are perturbed under pressure. The ⁷F₀→⁷F₄ (9615 cm⁻¹) transition shows slight peak broadening with increasing pressure and has a shift of -4 cm⁻¹/GPa. The ⁷F₀→⁷F₆ (12269 cm⁻¹) transition shows some broadening as the pressure increases, and a shift of -13 cm⁻¹/GPa. The ⁷F₀→⁵L₆ (19762 cm⁻¹) transition has a shifting of -9 cm⁻¹/GPa and broadens with increasing pressure. The ⁷F₀→⁵G₂ (22075 cm⁻¹) transition shifts by -14 cm⁻¹/GPa and broadens significantly with increasing pressure. This shift is less pronounced than what is seen for other Am^{III} compounds under applied pressure, such as the Am^{III} mellitate, Am₂[(C₆(CO₂)₆)(H₂O)₈·2H₂O], with the ⁷F₀→⁵L₆ transition having an average shift of -18 cm⁻¹/GPa; whereas **Am1** has an average shift of -9 cm⁻¹/GPa.⁵¹ In stark contrast, [Cm(pydtc)₄]¹⁻ (pydtc= pyrrolidinedithiocarbamate) has bathochromic peak shifts between 180 cm⁻¹ and 245 cm⁻¹ at 4 GPa. In the case of the Cm^{III} mellitate, Cm₂[(C₆(CO₂)₆)(H₂O)₈·2H₂O], small bathochromic shifts of the *f*→*f* transitions that are less than 130 cm⁻¹ up to 7 GPa are observed.

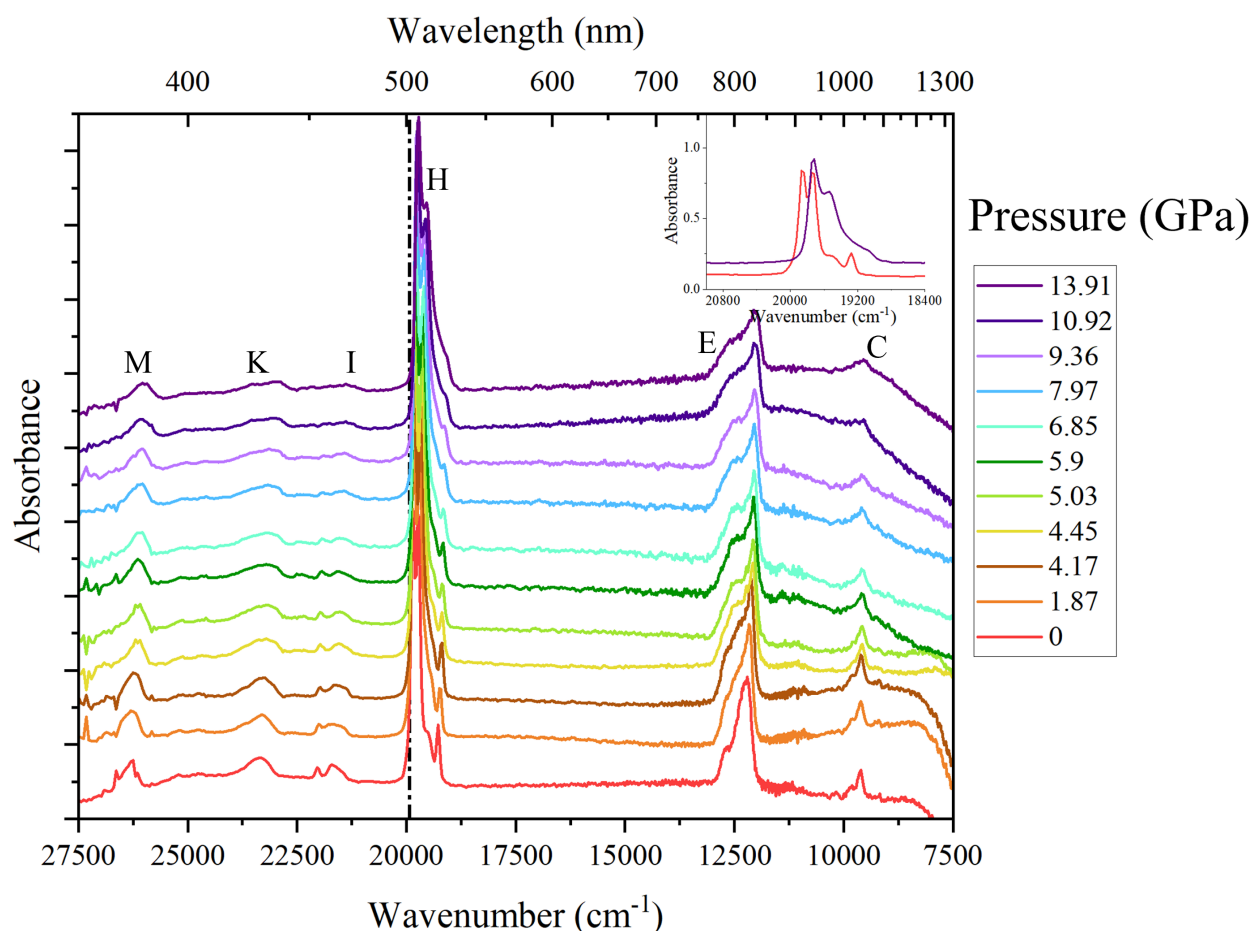


Figure 5. Variable-pressure UV-vis-NIR spectra of $\text{K}_2[\text{Am}(\text{OPS}(\text{OEt})_2)_5(\text{H}_2\text{O})_2] \cdot \text{CH}_2\text{Cl}_2 \cdot \text{H}_2\text{O}$ (**Am1**) with a straight dashed line at 504 nm and (inset) a comparison of the initial and final pressure showing the peak shifting and broadening.

For **Nd1**, (see Figure S8) the hypersensitive transition ${}^4\text{I}_{9/2} \rightarrow ({}^4\text{G}_{5/2})$ (580 nm) is perturbed under pressure with a shift of $-11 \text{ cm}^{-1}/\text{GPa}$. Other transitions such as the peaks at 514 nm, 747 nm and 803 nm are altered as well, but the lines are too broad and unclear to determine their corresponding shift. Overall, the **Am1** $5f \rightarrow 5f$ transitions shift to a slightly greater extent per GPa compared to **Nd1**. Thus, the predictions concerning the nature of the Am-S interactions are verified by these measurements, and the pressure response of $[\text{Am}(\text{OPS}(\text{OEt})_2)_5(\text{H}_2\text{O})_2]^{2-}$ and

$[\text{Nd}(\text{OPS}(\text{OEt})_2)_5(\text{H}_2\text{O})_2]^{2-}$ is much more similar to one another than $[\text{Am}(\text{OPS}(\text{OEt})_2)_5(\text{H}_2\text{O})_2]^{2-}$ is to $[\text{Cm}(\text{pydtc})_4]^{1-}$.

Conclusions

The crystallographic data, pressure-induced spectroscopic changes, and deviations in bond length obtained for $\text{K}_2[\text{Am}(\text{OPS}(\text{OEt})_2)_5(\text{H}_2\text{O})_2] \cdot \text{CH}_2\text{Cl}_2 \cdot \text{H}_2\text{O}$ (**Am1**) and $\text{K}_2[\text{Nd}(\text{OPS}(\text{OEt})_2)_5(\text{H}_2\text{O})_2] \cdot \text{CH}_2\text{Cl}_2 \cdot \text{H}_2\text{O}$ (**Nd1**) suggest that the interactions between sulfur donors with actinide ions have a slightly larger covalent contribution to bonding than found with lanthanides. In particular, the Am–S bond in $[\text{Am}(\text{OPS}(\text{OEt})_2)_5(\text{H}_2\text{O})_2]^{2-}$ (2.975(3) Å) is statistically shorter than the Nd–S bond in $[\text{Nd}(\text{OPS}(\text{OEt})_2)_5(\text{H}_2\text{O})_2]^{2-}$ (3.000(2) Å) even though Am(III) and Nd(III) possess overlapping ionic radii (1.108(4) Å and 1.107 Å, respectively). High pressure studies show that the nature of the interaction between the monothiophosphate and dithiophosphate sulfur donors are quite different from one another.

Supporting Information

Synthetic photographs, supplementary pressure data, crystallographic data, spectroscopic data, and additional characterization.

Accession Codes

CCDC 2301779 and 2301780 contain the supplementary crystallographic data for this paper. These data can be obtained free of charge via www.ccdc.cam.ac.uk/data_request/cif, or by emailing data_request@ccdc.cam.ac.uk, or by contacting The Cambridge Crystallographic Data Centre, 12 Union Road, Cambridge CB2 1EZ, UK; fax: +44 1223 336033.

Author Information

Corresponding Author:

Thomas E. Albrecht-Schönzart – Department of Chemistry and Nuclear Science & Engineering Center, Colorado School of Mines, Golden, Colorado 80401, United States; orcid.org/0000-0002-2989-3311,

Email: tschoenzart@mines.edu

Authors:

Daniela Gomez Martinez – Department of Chemistry and Nuclear Science and Engineering Center, Colorado School of Mines, Golden, CO 80401, USA; <https://orcid.org/0000-0003-1605-3409>

Joseph M. Sperling – Department of Chemistry and Nuclear Science and Engineering Center, Colorado School of Mines, Golden, CO 80401, USA; <https://orcid.org/0000-0003-1916-5633>

Nicholas B. Beck – Department of Chemistry and Nuclear Science and Engineering Center, Colorado School of Mines, Golden, CO 80401, USA; <https://orcid.org/0000-0001-5687-192X>

Hannah B. Wineinger – Department of Chemistry and Nuclear Science and Engineering Center, Colorado School of Mines, Golden, CO 80401, USA; <https://orcid.org/0000-0003-4070-999X>

Jacob P. Brannon – Department of Chemistry and Nuclear Science and Engineering Center, Colorado School of Mines, Golden, CO 80401, USA; <https://orcid.org/0000-0001-7786-127X>

Megan A. Whitefoot – Department of Chemistry and Nuclear Science and Engineering Center, Colorado School of Mines, Golden, CO 80401, USA; <https://orcid.org/0000-0001-8765-9542>

Gregory P. Horne – Center for Radiation Chemistry Research, Idaho National Laboratory, Idaho Falls, ID, P.O. Box 1625, 83415, USA; <https://orcid.org/0000-0003-0596-0660>

Notes

The authors declare no competing financial interest.

Acknowledgements

This material is based upon work supported by the U.S Department of Energy, Office of Science, Office of Basic Energy Sciences, Solar Photochemistry Program, under the Award Number DE-SC0024191. The isotopes used in this research were supplied by the U.S. Department of Energy, Office of Science, by the Isotope Program in the Office of Nuclear Physics. The ^{243}Am was provided by the Isotope Development and Production for Research and Applications Program through the Radiochemical Engineering and Development Center at Oak Ridge National Laboratory.

References

- (1) Grimes, R. W.; Nuttall, W. J. Generating the Option of a Two-Stage Nuclear Renaissance. *Science* **2010**, 329 (5993), 799–803. <https://doi.org/10.1126/science.1188928>.
- (2) Roberto, J. B.; de la Rubia, T. D. Basic Research Needs for Advanced Nuclear Energy Systems. *JOM* **2007**, 59 (4), 16–19. <https://doi.org/10.1007/s11837-007-0048-x>.
- (3) Vértes, A.; Nagy, S.; Klencsár, Z.; Lovas, R. G. Options in the Fuel Cycle That Impact Waste Management. In *Handbook Of Nuclear Chemistry, 2nd Edition*; 2010; p 3049.
- (4) U.S. Department of Energy's Waste Isolation Pilot Plant - WIPP Site. <https://wipp.energy.gov/wipp-site.asp> (accessed 2023-11-03).
- (5) Madic, C.; Bourges, J.; Dozol, J. Brief Overview of the Long-lived Radionuclide Separation Processes Developed in France in Connection with the Spin Program. *AIP Conf. Proc.* **1995**, 346 (1), 628–638. <https://doi.org/10.1063/1.49144>.
- (6) Burns, J. D.; Shehee, T. C.; Clearfield, A.; Hobbs, D. T. Separation of Americium from Curium by Oxidation and Ion Exchange. *Anal. Chem.* **2012**, 84 (16), 6930–6932. <https://doi.org/10.1021/ac3018394>.
- (7) Moyer, B. A. *Ion Exchange and Solvent Extraction: A Series of Advances, Volume 19*; CRC Press, 2009.
- (8) Ewing, R. C. Safe Management of Actinides in the Nuclear Fuel Cycle: Role of Mineralogy. *Comptes Rendus Geosci.* **2011**, 343 (2), 219–229. <https://doi.org/10.1016/j.crte.2010.09.003>.
- (9) Vidanov, V. L.; Shadrin, A. Yu.; Tkachenko, L. I.; Kenf, E. V.; Parabin, P. V.; Shirokov, S. S. Separation of Americium and Curium for Transmutation in the Fast Neutron Reactor. *Nucl. Eng. Des.* **2021**, 385, 111434. <https://doi.org/10.1016/j.nucengdes.2021.111434>.
- (10) Gelis, A. V.; Lumetta, G. J. Actinide Lanthanide Separation Process—ALSEP. *Ind. Eng. Chem. Res.* **2014**, 53 (4), 1624–1631. <https://doi.org/10.1021/ie403569e>.
- (11) Campbell, D. O.; Buxton, S. R. *Recovery of Americium and Curium from Nuclear Fuel Processing Waste Solutions*; CONF-760826-8; Oak Ridge National Lab., Tenn. (USA), 1976. <https://www.osti.gov/biblio/7338455> (accessed 2024-01-26).

- (12) Alyapyshev, M. Y.; Babain, V. A.; Ustynyuk, Y. A. Recovery of Minor Actinides from High-Level Wastes: Modern Trends. *Russ. Chem. Rev.* **2016**, *85* (9), 943. <https://doi.org/10.1070/RCR4589>.
- (13) Burger, L. L. *The Chemistry of Tributyl Phosphate: A Review*; HW-40910; General Electric Co. Hanford Atomic Products Operation, Richland, Wash., 1955. <https://doi.org/10.2172/4334996>.
- (14) Burger, L. L. Uranium and Plutonium Extraction by Organophosphorus Compounds. *J. Phys. Chem.* **1958**, *62* (5), 590–593. <https://doi.org/10.1021/j150563a017>.
- (15) Hudson, M. J.; Harwood, L. M.; Laventine, D. M.; Lewis, F. W. Use of Soft Heterocyclic N-Donor Ligands to Separate Actinides and Lanthanides. *Inorg. Chem.* **2013**, *52* (7), 3414–3428. <https://doi.org/10.1021/ic3008848>.
- (16) Lewis, F.; Hudson, M.; Harwood, L. Development of Highly Selective Ligands for Separations of Actinides from Lanthanides in the Nuclear Fuel Cycle. *Synlett* **2011**, *2011* (18), 2609–2632. <https://doi.org/10.1055/s-0030-1289557>.
- (17) Ensor, D. D.; Jarvinen, G. D.; Smith, B. F. The Use of Soft Donor Ligands, 4-Benzoyl-2,4-Dihydro-5-Methyl-2-Phenyl-3h-Pyrazol-3-Thione and 4,7-Diphenyl-Uo-Phenanthroline, for Improved Separation of Trivalent Americium and Europium. *Solvent Extr. Ion Exch.* **1988**, *6* (3), 439–445. <https://doi.org/10.1080/07366298808917948>.
- (18) Moyer, B. A. Overview of Solvent Extraction Chemistry for Reprocessing. In *Ion Exchange and Solvent Extraction: A Series of Advances, Volume 19*; CRC Press, 2009.
- (19) Bhattacharyya, A.; Mohapatra, P. K.; Manchanda, V. K. Role of Ligand Softness and Diluent on the Separation Behaviour of Am(III) and Eu(III). *J. Radioanal. Nucl. Chem.* **2011**, *288* (3), 709–716. <https://doi.org/10.1007/s10967-011-1027-9>.
- (20) Nash, K. L. A Review of the Basic Chemistry and Recent Developments in Trivalent F-Elements Separations. *Solvent Extr. Ion Exch.* **1993**, *11* (4), 729–768. <https://doi.org/10.1080/07366299308918184>.
- (21) Sadhu, B.; Dolg, M. Enhancing Actinide(III) over Lanthanide(III) Selectivity through Hard-by-Soft Donor Substitution: Exploitation and Implication of Near-Degeneracy-Driven Covalency. *Inorg. Chem.* **2019**, *58* (15), 9738–9748. <https://doi.org/10.1021/acs.inorgchem.9b00705>.
- (22) Weaver, B.; Kappelmann, F. A. *Talspeak: A New Method of Separating Americium and Curium from the Lanthanides by Extraction from an Aqueous Solution of an Aminopolyacetic Acid Complex with a Monoacidic Organophosphate or Phosphonate*; ORNL-3559, 4028257; 1964; p ORNL-3559, 4028257. <https://doi.org/10.2172/4028257>.
- (23) Kaneko, M.; Miyashita, S.; Nakashima, S. Bonding Study on the Chemical Separation of Am(III) from Eu(III) by S-, N-, and O-Donor Ligands by Means of All-Electron ZORA-DFT Calculation. *Inorg. Chem.* **2015**, *54* (14), 7103–7109. <https://doi.org/10.1021/acs.inorgchem.5b01204>.
- (24) Bhattacharyya, A.; Mohapatra, P. K. Separation of Trivalent Actinides and Lanthanides Using Various 'N', 'S' and Mixed 'N,O' Donor Ligands: A Review. *Radiochim. Acta* **2019**, *107* (9–11), 931–949. <https://doi.org/10.1515/ract-2018-3064>.
- (25) Leoncini, A.; Huskens, J.; Verboom, W. Ligands for F-Element Extraction Used in the Nuclear Fuel Cycle. *Chem. Soc. Rev.* **2017**, *46* (23), 7229–7273. <https://doi.org/10.1039/C7CS00574A>.
- (26) Jarvinen, G. D.; Barrans, R. E.; Schroeder, N. C.; Wade, K. L.; Jones, M. M.; Smith, B. F.; Mills, J. L.; Howard, G.; Freiser, H.; Muralidharan, S. Selective Extraction of Trivalent Actinides from Lanthanides with Dithiophosphinic Acids and Tributylphosphate. In *Separations of f Elements*; Nash, K. L., Choppin, G. R., Eds.; Springer US: Boston, MA, 1995; pp 43–62. https://doi.org/10.1007/978-1-4899-1406-4_5.
- (27) Zhu, Y.; Chen, J.; Jiao, R. Extraction of Am(III) and Eu(III) from Nitrate Solution with Purified Cyanex 301. *Solvent Extr. Ion Exch.* **1996**, *14* (1), 61–68.

<https://doi.org/10.1080/07366299608918326>.

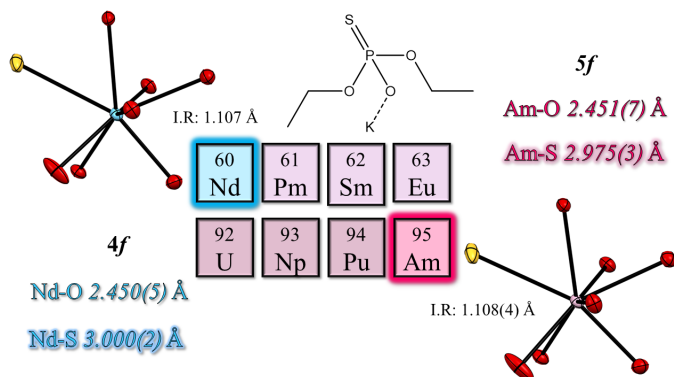
- (28) Peters, G. Reactions of Secondary Phosphine Sulfides. *J. Org. Chem.* **1962**, *27* (6), 2198–2201. <https://doi.org/10.1021/jo01053a074>.
- (29) Greer, R. D. M.; Celis-Barros, C.; Sperling, J. M.; Gaiser, A. N.; Windorff, C. J.; Albrecht-Schönzart, T. E. Structure and Characterization of an Americium Bis(O,O'-Diethyl)Dithiophosphate Complex. *Inorg. Chem.* **2020**, *59* (22), 16291–16300. <https://doi.org/10.1021/acs.inorgchem.0c02085>.
- (30) Pinkerton, A. A.; Schwarzenbach, D. Crystal and Molecular Structures of $[\text{AsPh}_4][\text{Ln}\{\text{S}_2\text{P}(\text{OEt})_2\}_4]$ (Ln = La or Er) and Their Comparison with Results Obtained in Solution from Paramagnetic Nuclear Magnetic Resonance Data. *J. Chem. Soc. Dalton Trans.* **1981**, No. 7, 1470–1474. <https://doi.org/10.1039/DT9810001470>.
- (31) Pinkerton, A. A.; Schwarzenbach, D. Ligand Displacement from Tetrakis(O,O'-Diethyl Phosphorodithioate)-Lanthanoid(III) Anions by Triphenylphosphine Oxide. X-Ray Crystal Structure of $[\text{La}\{\text{S}_2\text{P}(\text{OEt})_2\}_3(\text{POPh}_3)_2]$ and $[\text{Sm}\{\text{S}_2\text{P}(\text{OEt})_2\}_2(\text{POPh}_3)_3][\text{S}_2\text{P}(\text{OEt})_2]$. *J. Chem. Soc. Dalton Trans.* **1976**, No. 23, 2466–2471. <https://doi.org/10.1039/DT9760002466>.
- (32) Mühlisepfen, K.-M.; Mattes, R. Thiophosphinatokomplexe der Lanthanoiden. II. Dicyclohexylthiophosphinatokomplexe des NdIII und ErIII. *Z. Für Anorg. Allg. Chem.* **1983**, *506* (11), 125–132. <https://doi.org/10.1002/zaac.19835061114>.
- (33) Mühlisepfen, K.-M.; Mattes, R. Thiophosphinatokomplexe der Lanthanoiden. I. Dimere Dimethylthiophosphinatokomplexe des LaIII, PrIII, NdIII und ErIII. *Z. Für Anorg. Allg. Chem.* **1983**, *506* (11), 115–124. <https://doi.org/10.1002/zaac.19835061113>.
- (34) Mattes, R.; Nieland, L. Synthesis of Thorium(IV)Thiophosphinates. Structure of $[\text{Th}(\text{Ph}_2\text{P}(\text{S})\text{O})_4(\text{EtOH})_4](\text{CH}_2\text{Cl}_2)_2$. *Inorganica Chim. Acta* **1986**, *112* (2), 215–217. [https://doi.org/10.1016/S0020-1693\(00\)84500-4](https://doi.org/10.1016/S0020-1693(00)84500-4).
- (35) Greiwing, H.; Krebs, B.; Pinkerton, A. A. An Unusual Reduction of Uranyl Ion to Uranium(IV). *Inorganica Chim. Acta* **1995**, *234* (1), 127–130. [https://doi.org/10.1016/0020-1693\(95\)04612-D](https://doi.org/10.1016/0020-1693(95)04612-D).
- (36) Echizen, T.; Ibrahim, M. M.; Nakata, K.; Izumi, M.; Ichikawa, K.; Shiro, M. Nucleophilic Reaction by Carbonic Anhydrase Model Zinc Compound: Characterization of Intermediates for CO₂ Hydration and Phosphoester Hydrolysis. *J. Inorg. Biochem.* **2004**, *98* (8), 1347–1360. <https://doi.org/10.1016/j.jinorgbio.2004.04.022>.
- (37) Ibrahim, M. M.; Ichikawa, K.; Shiro, M. Solution Studies of N',N'',N'''-Tris(3-Aminopropyl)Amine-Based Zinc(II) Complexes and X-Ray Crystal Structures of $[\text{Zn}(\text{Trpn})](\text{ClO}_4)_2$ and $[\text{Zn}(\text{Trpn})(\text{DETP})]\text{ClO}_4$, DETP=O,O-Diethyl Thiophosphate. Catalytic Activity of the Complexes in the Hydrolysis of the Phosphotriester 2,4-Dinitrophenyl Diethyl Phosphate. *Inorganica Chim. Acta* **2003**, *353*, 187–196. [https://doi.org/10.1016/S0020-1693\(03\)00239-1](https://doi.org/10.1016/S0020-1693(03)00239-1).
- (38) Lu, S.-F.; Huang, M.-D.; Huang, J.-Q.; Huang, Z.-X.; Huang, J.-L. Structure of Tris(Diethyldithiophosphato-S,S')- μ -(Diethylthiophosphate-O,S)-(Oxazole)- μ_3 -Sulfido-Tri- μ_2 -Sulfido-Cyclo-Trimolybdenum(3 Mo–Mo). *Acta Crystallogr. C* **1990**, *46* (11), 2036–2039. <https://doi.org/10.1107/S0108270190001299>.
- (39) Ross, S. A.; Lowe, G.; Watkin, D. J. (4'-Chloro-2,2':6',2''-Terpyridine-N,N',N'')(Diethylphosphinothioato-S)Platinum(II) Tetraphenylborate. *Acta Crystallogr. C* **2001**, *57* (3), 275–276. <https://doi.org/10.1107/S0108270100020023>.
- (40) Cary, S. K.; Su, J.; Galley, S. S.; Albrecht-Schmitt, T. E.; Batista, E. R.; Ferrier, M. G.; Kozimor, S. A.; Mocko, V.; Scott, B. L.; Alstine, C. E. V.; White, F. D.; Yang, P. A Series of Dithiocarbamates for Americium, Curium, and Californium. *Dalton Trans.* **2018**, *47* (41), 14452–14461. <https://doi.org/10.1039/C8DT02658K>.
- (41) Sheldrick, G. M. SHELXT – Integrated Space-Group and Crystal-Structure Determination.

- Acta Crystallogr. Sect. Found. Adv.* **2015**, *71* (1), 3–8. <https://doi.org/10.1107/S2053273314026370>.
- (42) Dolomanov, O. V.; Bourhis, L. J.; Gildea, R. J.; Howard, J. a. K.; Puschmann, H. OLEX2: A Complete Structure Solution, Refinement and Analysis Program. *J. Appl. Crystallogr.* **2009**, *42* (2), 339–341. <https://doi.org/10.1107/S0021889808042726>.
- (43) Milburn, G. International Tables for X-Ray Crystallography. *Structural Science* **1983**.
- (44) Chijioke, A. D.; Nellis, W. J.; Soldatov, A.; Silvera, I. F. The Ruby Pressure Standard to 150 GPa. *J. Appl. Phys.* **2005**, *98* (11), 114905. <https://doi.org/10.1063/1.2135877>.
- (45) Dewaele, A.; Torrent, M.; Loubeyre, P.; Mezouar, M. Compression Curves of Transition Metals in the Mbar Range: Experiments and Projector Augmented-Wave Calculations. *Phys. Rev. B* **2008**, *78* (10), 104102. <https://doi.org/10.1103/PhysRevB.78.104102>.
- (46) Fedosseev, A. M.; Grigoriev, M. S.; Budantseva, N. A.; Guillaumont, D.; Le Naour, C.; Simoni, É.; Den Auwer, C.; Moisy, P. Americium(III) Coordination Chemistry: An Unexplored Diversity of Structure and Bonding. *Comptes Rendus Chim.* **2010**, *13* (6), 839–848. <https://doi.org/10.1016/j.crci.2010.04.018>.
- (47) Cross, J. N.; Villa, E. M.; Wang, S.; Diwu, J.; Polinski, M. J.; Albrecht-Schmitt, T. E. Syntheses, Structures, and Spectroscopic Properties of Plutonium and Americium Phosphites and the Redetermination of the Ionic Radii of Pu(III) and Am(III). *Inorg. Chem.* **2012**, *51* (15), 8419–8424. <https://doi.org/10.1021/ic300958z>.
- (48) David, F. Thermodynamic Properties of Lanthanide and Actinide Ions in Aqueous Solution. *J. Common Met.* **1986**, *121*, 27–42. [https://doi.org/10.1016/0022-5088\(86\)90511-4](https://doi.org/10.1016/0022-5088(86)90511-4).
- (49) Long, B. N.; Beltrán-Leiva, M. J.; Celis-Barros, C.; Sperling, J. M.; Poe, T. N.; Baumbach, R. E.; Windorff, C. J.; Albrecht-Schönzart, T. E. Cyclopentadienyl Coordination Induces Unexpected Ionic Am–N Bonding in an Americium Bipyridyl Complex. *Nat. Commun.* **2022**, *13* (1), 201. <https://doi.org/10.1038/s41467-021-27821-4>.
- (50) Cross, J. N.; Macor, J. A.; Bertke, J. A.; Ferrier, M. G.; Girolami, G. S.; Kozimor, S. A.; Maassen, J. R.; Scott, B. L.; Shuh, D. K.; Stein, B. W.; Stieber, S. C. E. Comparing the 2,2'-Biphenylenedithiophosphinate Binding of Americium with Neodymium and Europium. *Angew. Chem. Int. Ed.* **2016**, *55* (41), 12755–12759. <https://doi.org/10.1002/anie.201606367>.
- (51) Sperling, J. M.; Warzecha, E.; Klamm, B. E.; Gaiser, A. N.; Windorff, C. J.; Whitefoot, M. A.; Albrecht-Schönzart, T. E. Pronounced Pressure Dependence of Electronic Transitions for Americium Compared to Isomorphous Neodymium and Samarium Mellitates. *Inorg. Chem.* **2021**, *60* (1), 476–483. <https://doi.org/10.1021/acs.inorgchem.0c03293>.
- (52) Windorff, C. J.; Celis-Barros, C.; Sperling, J. M.; McKinnon, N. C.; Albrecht-Schmitt, T. E. Probing a Variation of the Inverse-Trans-Influence in Americium and Lanthanide Tribromide Tris(Tricyclohexylphosphine Oxide) Complexes. *Chem. Sci.* **2020**, *11* (10), 2770–2782. <https://doi.org/10.1039/C9SC05268B>.
- (53) Corbey, J. F.; Rapko, B. M.; Wang, Z.; McNamara, B. K.; Surbella, R. G. I.; Pellegrini, K. L.; Schwantes, J. M. Crystallographic and Spectroscopic Characterization of Americium Complexes Containing the Bis[(Phosphino)Methyl]Pyridine-1-Oxide (NOPOPO) Ligand Platform. *Inorg. Chem.* **2018**, *57* (4), 2278–2287. <https://doi.org/10.1021/acs.inorgchem.7b03154>.
- (54) Dan, D.; Celis-Barros, C.; White, F. D.; Sperling, J. M.; Albrecht-Schmitt, T. E. Origin of Selectivity of a Triazinyl Ligand for Americium(III) over Neodymium(III). *Chem. – Eur. J.* **2019**, *25* (13), 3248–3252. <https://doi.org/10.1002/chem.201806070>.
- (55) Galley, S. S.; Pattenaude, S. A.; Gaggioli, C. A.; Qiao, Y.; Sperling, J. M.; Zeller, M.; Pakhira, S.; Mendoza-Cortes, J. L.; Schelter, E. J.; Albrecht-Schmitt, T. E.; Gagliardi, L.; Bart, S. C. Synthesis and Characterization of Tris-Chelate Complexes for Understanding f-Orbital Bonding in Later Actinides. *J. Am. Chem. Soc.* **2019**, *141* (6), 2356–2366. <https://doi.org/10.1021/jacs.8b10251>.
- (56) Danford, M. D.; Burns, J. H.; Higgins, C. E.; Stokely, J. R. Jr.; Baldwin, W. H. Preparation

- and Properties of Some Rare Earth and Americium Chelates. *Inorg. Chem.* **1970**, *9* (8), 1953–1955. <https://doi.org/10.1021/ic50090a044>.
- (57) Fedoseev, A. M.; Sokolova, M. N.; Grigor'ev, M. S.; Budantseva, N. A. New Compounds of Some Trivalent Lanthanides and Actinides with Furancarboxylic Acid. Synthesis, Structure, and Absorption Spectra of the Complexes $[(\text{NH}_2)_3\text{C}]_2[\text{M}(\text{OCC}_4\text{H}_3\text{O})_5]$ (M = La, Ce, Pr, Nd, Tb, Np, Pu, Am). *Radiochemistry* **2018**, *60* (6), 573–580. <https://doi.org/10.1134/S1066362218060024>.
- (58) Gogolev, A. V.; Grigoriev, M. S.; Budantseva, N. A.; Fedoseev, A. M. Structure and Properties of 2,2-Dihydroxymalonates of Trivalent Y, Lanthanides, Pu and Am. *Russ. J. Coord. Chem.* **2013**, *39* (3), 271–277. <https://doi.org/10.1134/S1070328413030032>.
- (59) Wilson, R. E.; Carter, T. J.; Autillo, M.; Stegman, S. Thiocyanate Complexes of the Lanthanides, Am and Cm. *Chem. Commun.* **2020**, *56* (17), 2622–2625. <https://doi.org/10.1039/C9CC07612C>.
- (60) Charushnikova, I. A.; Fedoseev, A. M.; Perminov, V. P. Synthesis and Structure of Complex Nitrates of Some Ln(III) and of Am(III) with 1,10-Phenanthroline-2,9-Dicarboxylic Acid Anions. *Radiochemistry* **2015**, *57* (2), 111–121. <https://doi.org/10.1134/S1066362215020010>.
- (61) Tamain, C.; Arab-Chapelet, B.; Rivenet, M.; Legoff, X. F.; Loubert, G.; Grandjean, S.; Abraham, F. Coordination Modes of Americium in the $\text{Am}_2(\text{C}_2\text{O}_4)_3(\text{H}_2\text{O})_6 \cdot 4\text{H}_2\text{O}$ Oxalate: Synthesis, Crystal Structure, Spectroscopic Characterizations and Comparison in the $\text{M}_2(\text{C}_2\text{O}_4)_3(\text{H}_2\text{O})_6 \cdot n\text{H}_2\text{O}$ (M = Ln, An) Series. *Inorg. Chem.* **2016**, *55* (1), 51–61. <https://doi.org/10.1021/acs.inorgchem.5b01781>.
- (62) Huffman, Z. K.; Sperling, J. M.; Windorff, C. J.; Long, B. N.; Cordova, L.; Ramanantoanina, H.; Celis-Barros, C.; Albrecht-Schönzart, T. E. Synthesis and Characterization of a Bimetallic Americium(III) Pyrrithionate Coordination Complex. *Chem. Commun.* **2022**, *58* (84), 11791–11794. <https://doi.org/10.1039/D2CC03352F>.
- (63) Casanova, D.; Lluell, M.; Alemany, P.; Alvarez, S. The Rich Stereochemistry of Eight-Vertex Polyhedra: A Continuous Shape Measures Study. *Chem. – Eur. J.* **2005**, *11* (5), 1479–1494. <https://doi.org/10.1002/chem.200400799>.
- (64) Grigoriev, M. S.; Fedoseev, A. M.; Moisy, Ph. *Frumkin Inst. Phys. Chem. Electrochem. RAS* **2019**, No. 72.
- (65) Prüßmann, T.; Denecke, M. A.; Geist, A.; Rothe, J.; Lindqvist-Reis, P.; Löble, M.; Breher, F.; Batchelor, D. R.; Apostolidis, C.; Walter, O.; Caliebe, W.; Kvashnina, K.; Jorissen, K.; Kas, J. J.; Rehr, J. J.; Vitova, T. Comparative Investigation of N Donor Ligand-Lanthanide Complexes from the Metal and Ligand Point of View. *J. Phys. Conf. Ser.* **2013**, *430*, 012115. <https://doi.org/10.1088/1742-6596/430/1/012115>.
- (66) Pappalardo, R. G.; Carnall, W. T.; Fields, P. R. Low-Temperature Optical Absorption of Americium Halides. *J. Chem. Phys.* **1969**, *51* (3), 1182–1200. <https://doi.org/10.1063/1.1672121>.
- (67) Stephanou, S. E.; Nigon, J. P.; Penneman, R. A. The Solution Absorption Spectra of Americium(III), (V), and (VI). *J. Chem. Phys.* **1953**, *21* (1), 42–45. <https://doi.org/10.1063/1.1698619>.
- (68) Carnall, W. T.; Fields, P. R.; Rajnak, K. Electronic Energy Levels in the Trivalent Lanthanide Aquo Ions. I. Pr^{3+} , Nd^{3+} , Pm^{3+} , Sm^{3+} , Dy^{3+} , Ho^{3+} , Er^{3+} , and Tm^{3+} . *J. Chem. Phys.* **1968**, *49* (10), 4424–4442. <https://doi.org/10.1063/1.1669893>.
- (69) Henrie, D. E.; Fellows, R. L.; Choppin, G. R. Hypersensitivity in the Electronic Transitions of Lanthanide and Actinide Complexes. *Coord. Chem. Rev.* **1976**, *18* (2), 199–224. [https://doi.org/10.1016/S0010-8545\(00\)82044-5](https://doi.org/10.1016/S0010-8545(00)82044-5).
- (70) Wietzke, R.; Mazzanti, M.; Latour, J.-M.; Pécaut, J. Crystal Structure and Solution Fluxionality of Lanthanide Complexes of 2,4,6,-Tris-2-Pyridyl-1,3,5-Triazine. *Inorg. Chem.* **1999**, *38* (15), 3581–3585. <https://doi.org/10.1021/ic990122w>.
- (71) Wilharm, R. K.; Ramakrishnam Raju, M. V.; Hoefler, J. C.; Platas-Iglesias, C.; Pierre, V. C. Exploiting the Fluxionality of Lanthanide Complexes in the Design of Paramagnetic Fluorine Probes.

- Inorg. Chem.* **2022**, *61* (9), 4130–4142. <https://doi.org/10.1021/acs.inorgchem.1c03908>.
- (72) Benedict, U.; Holzapfel, W. B. Chapter 113 High-Pressure Studies — Structural Aspects. In *Handbook on the Physics and Chemistry of Rare Earths*; Elsevier, 1993; Vol. 17, pp 245–300. [https://doi.org/10.1016/S0168-1273\(05\)80030-3](https://doi.org/10.1016/S0168-1273(05)80030-3).
- (73) Tröster, Th.; Gregorian, T.; Holzapfel, W. B. Energy Levels of Nd 3 + and Pr 3 + in R Cl 3 under Pressure. *Phys. Rev. B* **1993**, *48* (5), 2960–2967. <https://doi.org/10.1103/PhysRevB.48.2960>.
- (74) Sperling, J. M.; Warzecha, E. J.; Celis-Barros, C.; Sergentu, D.-C.; Wang, X.; Klamm, B. E.; Windorff, C. J.; Gaiser, A. N.; White, F. D.; Beery, D. A.; Chemey, A. T.; Whitefoot, M. A.; Long, B. N.; Hanson, K.; Kögerler, P.; Speldrich, M.; Zurek, E.; Autschbach, J.; Albrecht-Schönzart, T. E. Compression of Curium Pyrrolidine-Dithiocarbamate Enhances Covalency. *Nature* **2020**, *583* (7816), 396–399. <https://doi.org/10.1038/s41586-020-2479-2>.

TOC



The separation of lanthanides from actinides can be accomplished through the use of soft-donor extractants that can degrade to mixed oxygen/sulfur ligand such as monothiophosphates via hydrolysis and radiolysis. To understand potential differences between the binding of such ligands to Nd^{3+} and Am^{3+} , the monothiophosphate complexes $[\text{M}(\text{OPS}(\text{OEt})_2)_5(\text{H}_2\text{O})_2]^{2-}$ ($\text{M}^{3+} = \text{Nd}^{3+}, \text{Am}^{3+}$) were prepared, characterized, and studied as a function of pressure up ca. 14 GPa using diamond-anvil techniques.